A Sensorless, Stable V/f Control Method for Permanent-Magnet Synchronous Motor Drives

P. D. Chandana Perera, *Student Member, IEEE*, Frede Blaabjerg, *Fellow, IEEE*, John K. Pedersen, *Senior Member, IEEE*, and Paul Thøgersen, *Senior Member, IEEE*

***Abstract*—When permanent-magnet synchronous motors (PMSMs) are used for pump and fan applications, V/f control methods can be used to control them. The problem with open-loop V/f control of PMSMs without having damper windings in the rotor is the inherent instability after exceeding a certain applied frequency. In this paper, a new V/f control method is proposed for motor drives for stable operation in a wide frequency range. The magnitude of the voltage is controlled in order to maintain a constant stator flux linkage in the PMSM. The applied frequency is modulated proportional to the input power perturbations to stabilize the drive for a wide frequency range. No position sensor is required to implement this stabilizing technique. The small-signal analysis and the experimental results confirm the effectiveness of this stabilizing technique. The experimental results also indicate the satisfactory performance of the drive for pump and fan applications.**

***Index Terms*—Permanent-magnet synchronous motor (PMSM), sensorless control, synchronous motor stability, volts-per-hertz (V/f) control.**

I. Introduction

THERE IS A WIDE appeal for permanent-magnet synchronous motors (PMSMs) in motion control applications due to their attractive features such as high efficiency and high power density [1]–[3]. For high-performance motion control applications, like servo applications, the closed-loop control with field orientation should be incorporated with those machines to achieve high dynamic performance in position, speed, and torque control [2]–[4]. The knowledge of rotor position and rotor speed is essential for those field-oriented-controlled PMSM drive systems and they should be estimated accurately for sensorless control of them [5]–[7]. However, when PMSM drives are used for applications like pumps and fans, where high dynamic performance is not a demand, a simple V/f control strategy can be used instead of the sensorless field-oriented-control approach.

The interior-type PMSMs, which are designed with damper windings in the rotor, can be used for open-loop V/f control as shown in Fig. 1 for pump and fan applications [2]. The existence of the damper windings in the rotor assures the synchronization of motion of the rotor with the stator applied frequency, which is the fundamental requirement for synchronous machine control. This allows a stable control of this type of PMSM in an open-loop manner as shown in Fig. 1.

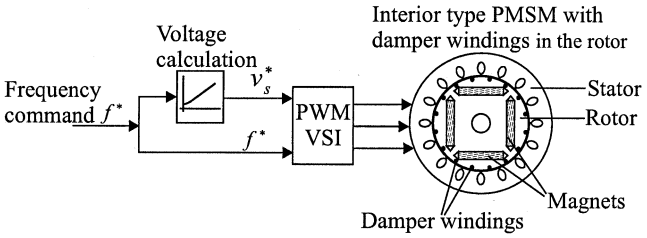

Fig. 1. Open-loop V/f control approach, which can be used for interior-type PMSMs with damper windings in the rotor.

Due to the high manufacturing cost and the difficulty to design rotors with damper windings for some type of PMSMs (e.g., surface-mounted-type PMSMs), the PMSMs are not generally available with damper windings in the rotor. The PMSMs without damper windings in the rotor do not assure the synchronization of motion of the rotor with stator applied frequency under the open-loop V/f control approach shown in Fig. 1. This causes instability problems in those PMSMs under the open-loop V/f control approach and an additional signal is required to the V/f controller in order to assure the synchronization and the stable operation.

In [8]–[10], the perturbations in the dc-link current have been used to modulate the applied frequency in the V/f controller in order to achieve stable operation of a PMSM without having damper windings in the rotor. In [8] and [10], the voltage has been controlled by incorporating a search algorithm so that the power input to the PMSM is minimized, whereas in [9] the voltage has been controlled in order to achieve unity power factor. Even though the stability of the drive was improved with frequency modulation, the low-speed performance of the drive was not at a satisfactory level in those V/f-controlled drive systems described in [8]–[10].

A stable i/f control method was proposed in [11] for a synchronous reluctance motor without damper windings in the rotor. The current control provides overcurrent protection and better starting performance in this drive compared to the V/f control approach. The stabilization of the drive was achieved by adjusting the current amplitude according to the power-factor angle variation. However, there was no analytical model given to design this i/f controller.

Paper IPCSD 03–006, presented at the 2002 IEEE Applied Power Electronics Conference and Exposition, Dallas, TX, March 10–14, and approved for publication in the IEEE TRANSACTIONS ON INDUSTRY APPLICATIONS by the Industrial Drives Committee of the IEEE Industry Applications Society. Manuscript submitted for review August 1, 2002 and released for publication January 21, 2003.

P. D. Chandana Perera, F. Blaabjerg, and J. K. Pedersen are with the Institute of Energy Technology, Aalborg University, DK-9220 Aalborg East, Denmark (e-mail: cp@iet.auc.dk; fbl@iet.auc.dk; jkp@iet.auc.dk).

P. Thøgersen is with Danfoss Drives A/S, DK-6300 Graasten, Denmark (e-mail: paul_thogersen@danfoss.com).

Digital Object Identifier 10.1109/TIA.2003.810624

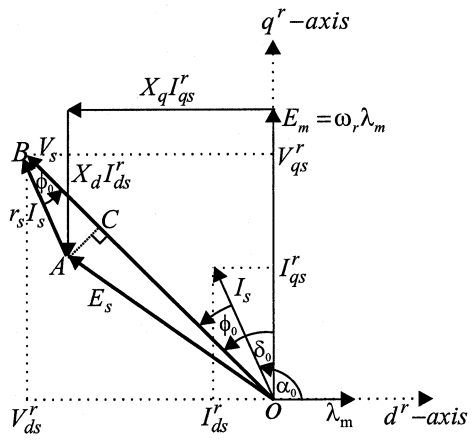

Fig. 2. Steady-state vector diagram of the PMSM showing the stator voltage vector as an addition of stator resistance voltage drop and induced voltage from the stator flux (in the triangle *OAB*).

In this paper, a new V/f control method incorporating a stabilizing technique is proposed for the PMSMs without damper windings in the rotor. A voltage control method in order to improve to the low-speed performance of the drive is first discussed, followed by the stability analysis of the drive. This leads to the discussion on stabilization of the drive. Using small-signal model analysis it will be shown that modulating the applied frequency proportional to the input power perturbations can add necessary damping and stabilize the drive for a wide frequency range operation. This is followed by experimental results to validate the control strategy.

II. Voltage Control Method and Stability Analysis

A. Voltage Control Method

In the proposed V/f control method, the magnitude of the voltage is calculated in order to maintain a constant stator flux linkage in the PMSM. With a constant stator flux linkage, the PMSM has the same torque-producing capability in all operating frequency ranges.

When calculating the magnitude of the voltage in order to maintain a constant stator flux linkage, the stator resistance voltage drop should also be compensated accurately and it is particularly important during low-speed operation [12]. The steady-state vector diagram of the PMSM shown in Fig. 2 can be used to explain the calculation of the voltage magnitude with vector compensation of the stator resistance voltage drop.

In the triangle *OAB* shown in Fig. 2, *AC* is drawn perpendicular to *OB*. From the *OAB* triangle the steady-state magnitude of the voltage vector V_s can be obtained as

$$V_s = BC + CO = I_s r_s \cos\phi_0 + \sqrt{E_s^2 - I_s^2 r_s^2 \sin^2\phi_0} \quad (1)$$

where I_s is the magnitude of the current vector, E_s is the magnitude of the voltage vector induced by stator flux linkage, and ϕ_0 is the power factor angle; all are in steady state. r_s is stator winding resistance per phase.

Using the trigonometric relationship $\sin^2\phi_0 + \cos^2\phi_0 = 1$, the magnitude of the voltage vector obtained in (1) can also be written as

$$V_s = I_s r_s \cos\phi_0 + \sqrt{E_s^2 + I_s^2 r_s^2 \cos^2\phi_0 - I_s^2 r_s^2}. \quad (2)$$

Equation (2) can be used to calculate the magnitude of the voltage command to the PMSM. The stator-flux-induced voltage E_s in (2), can be calculated from the required steady-state constant stator flux. The constant magnitude of the stator flux vector is selected as the rotor permanent-magnet flux λ_m. With this selection, the stator voltage requirement to the machine can be kept comparably low and the no-load current of the machine can be minimized. With this selection of the magnitude of the stator flux, E_s can be calculated as

$$E_s = 2\pi f_0 \lambda_m \quad (3)$$

where f_0 is the applied frequency to the machine.

Even though I_s and $\cos\phi_0$ are steady-state values, the instantaneously measured values of them can be used in (2) to command the magnitude of the voltage, so that the steady-state induced voltage from the stator flux will be the value given in (3). The term $I_s \cos\phi_0$ in (2) is the stator current vector component along with the stator voltage vector. By transforming the measured phase currents to the stator voltage fixed reference frame this term can instantaneously be calculated as

$$i_s \cos\phi = \frac{2}{3}\left[i_{as}\cos\theta_e + i_{bs}\cos\left(\theta_e - \frac{2\pi}{3}\right) - (i_{as} + i_{bs})\cos\left(\theta_e + \frac{2\pi}{3}\right)\right] \quad (4)$$

where i_s and ϕ are the instantaneous values of magnitude of the current vector and the power-factor angle, respectively. i_{as}, i_{bs} are measured phase currents and θ_e is the position of the voltage vector in the stationary reference frame.

i_s can also be obtained by measuring two phase currents and calculating the stationary d^s, q^s reference frame current components as given in (5)

$$i_s = \sqrt{(i_{ds}^s)^2 + (i_{qs}^s)^2} = \sqrt{\frac{1}{3}(i_{as} + 2i_{bs})^2 + (i_{as})^2}. \quad (5)$$

For both (4) and (5), the reference frame transformation equations described in [13] are used.

Using the instantaneously calculated values and the commanded value for E_s the final expression for calculation of magnitude of the voltage command v_s^* can be written as

$$v_s^* = (i_s \cos\phi) r_s + \sqrt{(2\pi f_0 \lambda_m)^2 + (i_s \cos\phi)^2 r_s^2 - i_s^2 r_s^2}. \quad (6)$$

Measuring the instantaneous currents the implementation of (6) in the drive system is shown in Fig. 3. To eliminate the high-frequency ripples in the calculated currents i_s and $i_s \cos\phi$, two low-pass filters (LPFs) are used as shown in Fig. 3.

The preliminary drive configuration with the above-discussed voltage control method is shown in Fig. 4.

The compensation of the inverter nonlinearities, i.e., dead time, voltage drop across the power devices, and ripple in the

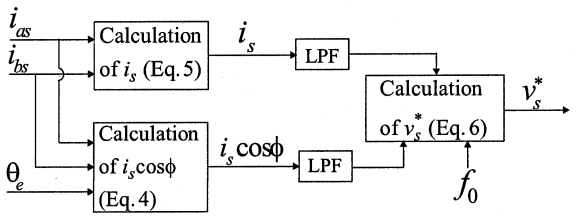

Fig. 3. Calculation of the voltage command.

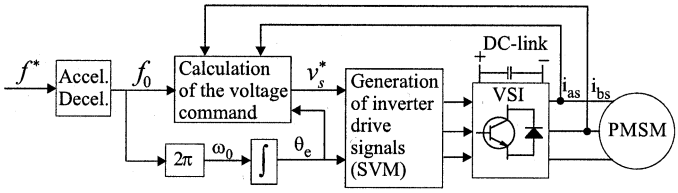

Fig. 4. Preliminary drive configuration with voltage control method.

dc-link voltage, is important in the voltage control. The detailed discussion of it goes beyond the scope of this paper and the implemented compensation methods can be found in [14].

For accurate compensation of stator resistance voltage drop, especially at low speeds, the variation of the stator resistance with temperature should also be considered in the voltage control algorithm. Since the present work is focused on pump and fan applications, where very high dynamic performance is not a demand at low speeds, the stator resistance variation with temperature is not considered in the voltage control algorithm.

Due to the absence of current control in the V/f control approach, the overcurrent protection does not inherently exist in the drive. However, when overcurrent is detected from phase current measurements the voltage and the frequency to the machine can be reduced until the current limit is reached, and then, they can be increased to the reference values again. In extreme situations, where the current limit cannot be achieved, the inverter can be stopped by switching off the transistors.

B. Stability Analysis

To analyze the stability of the PMSM under constant stator flux linkage control, the linearized PMSM model is used. The eigenvalues of the state transition matrix of the linearized PMSM model should show the stability behavior of the PMSM for the conditions under consideration [15], [16].

The state variable form of the rotor d^r, q^r frame equations of the PMSM without having damper windings in the rotor can be written as

$$pi_{qs}^r = \frac{-i_{qs}^r}{\sigma\tau_s} - \frac{\omega_r}{\sigma}\left(\frac{\lambda_m}{L_d} + i_{ds}^r\right) + \frac{v_s\cos(\delta)}{\sigma L_d} \tag{7}$$

$$pi_{ds}^r = \frac{-i_{ds}^r}{\tau_s} + \sigma\omega_r i_{qs}^r - \frac{v_s\sin(\delta)}{L_d} \tag{8}$$

$$p\omega_r = \frac{3}{2J}\left(\frac{n}{2}\right)^2\left[\lambda_m i_{qs}^r + L_d(1-\sigma)i_{qs}^r i_{ds}^r\right] - \frac{1}{J}B_m\omega_r - \frac{n}{2J}T_l \tag{9}$$

$$p\delta = \omega_e - \omega_r. \tag{10}$$

In (7)–(10),

$\tau_s = L_d/r_s$, $\sigma = L_q/L_d$;

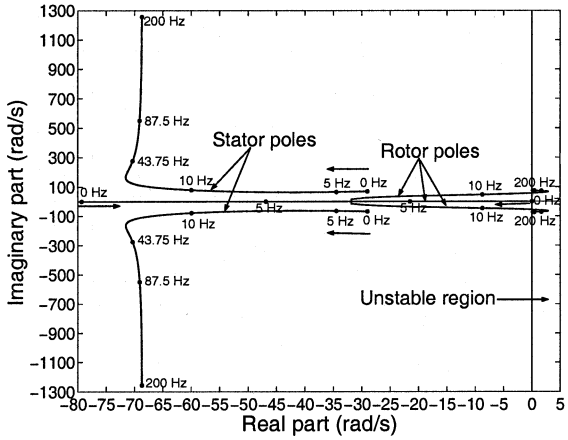

Fig. 5. Eigenvalue plot under no load, as a function of the applied frequency.

i_{qs}^r, i_{ds}^r rotor q^r- and d^r-axes currents;
L_q, L_d rotor q^r- and d^r-axes inductances;
p operator d/dt;
ω_r electrical rotor speed;
ω_e electrical speed of the applied voltage vector;
δ load angle;
J inertia of the motor and the load system;
B_m viscous friction coefficient;
n number of poles of the motor;
T_l load torque.

The machine state equations (7)–(10) have the form

$$\dot{x} = f(x,u) \tag{11}$$

where x is the vector of the machine state variables and f is the nonlinear function of the state x and the inputs u. The linearized system equations of this nonlinear system have the form

$$\dot{\Delta x} = A(X)\Delta x + B(X)\Delta u \tag{12}$$

where Δx is the perturbations matrix for state variables x, $A(X)$ is the state transition matrix, Δu is the input perturbation matrix, and $B(X)$ is the input matrix [16]. The derivation of the linearized machine equations is well discussed in [15] and [16]. The obtained linearized PMSM model can be written as in the matrix equation (13), shown at the bottom of the next page, which has the form given in (12). In (13), I_{qs}^r, I_{ds}^r, V_s, ω_0, and δ_0 represent the steady-state value of corresponding variable. When deriving this model, it is considered that the input voltage and the frequency to the PMSM are constant steady-state values, i.e., perturbations $\Delta v_s = 0$ and $\Delta\omega_e = 0$.

The state transition matrix $A(X)$ in (13) is determined by the machine parameters and the steady-state value of the machine variables (voltage, current, etc.). Using the constant stator flux linkage control strategy, the steady-state value of the machine variables can be calculated as described in Appendix I.

Fig. 5 shows the plot of the calculated eigenvalues of the state transition matrix $A(X)$ of (13), under no load, i.e., $V_s = E_m$ (back electomotive force (EMF) produced by rotor permanent magnets), as a function of the applied frequency. The PMSM used for these calculations is an interior-type one without damper windings in the rotor. The parameters are given in Appendix II.

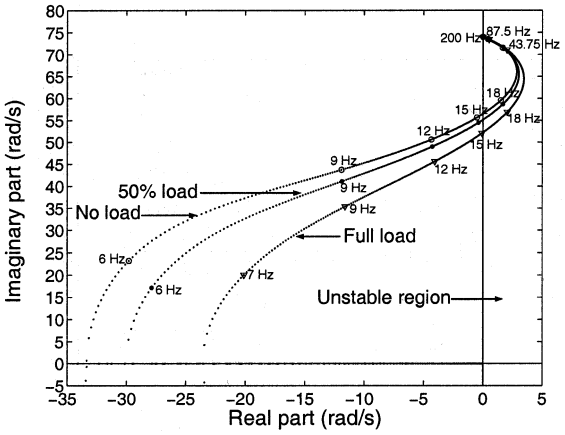

Fig. 6. Loci of the rotor poles under different load conditions, as a function of the applied frequency.

In Fig. 5, two types of machine poles are shown. One set of poles represents the fast-acting electrical dynamics in the stator of the PMSM, and they are referred to as "stator" poles. The other set represents the slow mechanical dynamics of the machine, and they are referred to as "rotor" poles. The important observation from Fig. 5 is the migration of the rotor poles to the unstable region of the s plane after exceeding the applied frequency by a certain value.

The eigenvalue plots drawn under load of the machine revealed that the basic shape of them is similar to the one shown in Fig. 5, which is drawn under no load. Fig. 6 shows the eigenvalue plots for different load conditions. For clarity, only the rotor poles (dominant poles) of the system are shown in Fig. 6.

As it can be observed from Fig. 6, the system becomes unstable (i.e., eigenvalues migrate into the right half of the s plane) after about 15 Hz under no-load or load conditions.

III. Stabilization of the Drive by Frequency Modulation

The PMSM's instability behavior after exceeding a certain applied frequency observed in Section II-B is due to the nonexistence of rotor circuits (i.e., damper windings) and, therefore, the weak coupling between electrical and mechanical modes of the machine. The stator and rotor poles move away from each other and, after exceeding a certain applied frequency, the slow rotor poles cross over to the instability region of the s plane, having a small positive real part. To stabilize the system for the whole applied frequency range, additional damping to the rotor poles is required in order to locate them in the stable region. This can be achieved by a proper modulation of the applied frequency of the machine.

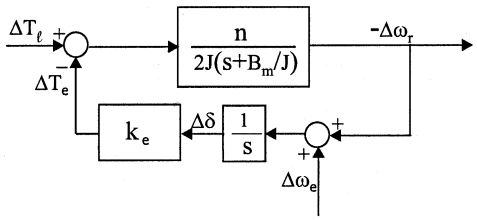

Fig. 7. Block diagram representation of the simplified small-signal dynamic model, which models only the rotor poles of the PMSM.

A. Simplified Small-Signal Dynamics Model Analysis

The insight of frequency modulation to add damping can be obtained from a simplified linearized model (simplified small-signal dynamics model) of the PMSM, which models only the rotor poles of the machine. This model in block diagram form is shown in Fig. 7. More details of this model can be found in [8] and [10].

The parameter k_e in Fig. 7 is the electromechanical spring constant and it is equal to the slope of the load-angle torque (δ–T_e) curve of the machine at the steady-state operating point [10], i.e.,

$$k_e = \frac{\partial T_e}{\partial \delta}|_{\delta_0}. \tag{14}$$

This simplified small-signal dynamics model and the power balance equation of the machine can be used to show how damping can be added to the system by modulating the applied frequency proportional to the perturbations of the input power of the machine.

The motor power balance equation can be written as

$$\begin{aligned} p_e &= P_e + \Delta p_e \\ &= p_{ml} + \frac{dw_{em}}{dt} + \left(\frac{2}{n}\right)^2 \frac{J}{2}\frac{d}{dt}\omega_r^2 + \left(\frac{2}{n}\right)^2 B_m \omega_r^2 + \frac{2}{n}\omega_r T_l \end{aligned} \tag{15}$$

where p_e is input power. P_e and Δp_e are the steady-state value and perturbation component of the input power, respectively. The input power is distributed among the motor losses p_{ml}, the

$$p\begin{bmatrix} \Delta i_{qs}^r \\ \Delta i_{ds}^r \\ \Delta \omega_r \\ \Delta \delta \end{bmatrix} = \underbrace{\begin{bmatrix} \frac{-1}{\sigma\tau_s} & \frac{-\omega_0}{\sigma} & \frac{-1}{\sigma}\left(\frac{\lambda_m}{L_d} + I_{ds}^r\right) & \frac{-V_s}{\sigma L_d}\sin(\delta_0) \\ \sigma\omega_0 & \frac{-1}{\tau_s} & \sigma I_{qs}^r & \frac{-V_s}{L_d}\cos(\delta_0) \\ \frac{3}{2}\left(\frac{n}{2}\right)^2 \frac{1}{J}[\lambda_m + L_d(1-\sigma)I_{ds}^r] & \frac{3}{2}\left(\frac{n}{2}\right)^2 \frac{1}{J} L_d(1-\sigma) I_{qs}^r & \frac{-B_m}{J} & 0 \\ 0 & 0 & -1 & 0 \end{bmatrix}}_{A(X)} \begin{bmatrix} \Delta i_{qs}^r \\ \Delta i_{ds}^r \\ \Delta \omega_r \\ \Delta \delta \end{bmatrix} + \begin{bmatrix} 0 \\ 0 \\ \frac{-n}{2J} \\ 0 \end{bmatrix} \Delta T_l \tag{13}$$

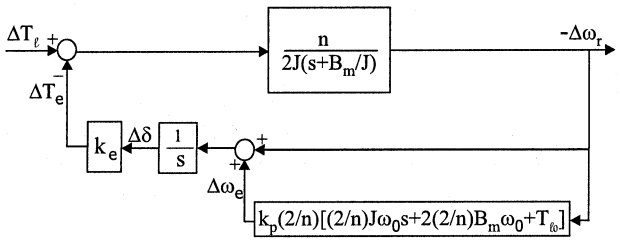

Fig. 8. Block diagram representation of the PMSM simplified small-signal dynamics when the applied frequency is modulated proportionally to the input power perturbations, i.e., $\Delta\omega_e = -k_p\Delta p_e$.

change in electromagnetic energy storage w_{em}, and the mechanical output power of the machine. From (15), it can be seen that the rotor velocity perturbations should mainly contribute to generate the power perturbations for an operating point. Therefore, the power perturbations are approximated coming from rotor velocity perturbations of the last three terms of (15). With this approximation the perturbations in the power can be written as

$$\Delta p_e = \left(\frac{2}{n}\right)^2 J\omega_0\frac{d}{dt}\Delta\omega_r + 2\left(\frac{2}{n}\right)^2 B_m\omega_0\Delta\omega_r + \frac{2}{n}T_{l0}\Delta\omega_r \tag{16}$$

where T_{l0} is the steady-state load torque. If the applied frequency is modulated proportionally to the power perturbations, then $\Delta\omega_e$ can be written as

$$\Delta\omega_e = -k_p\Delta p_e = k_p\left[\left(\frac{2}{n}\right)^2 J\omega_0\frac{d}{dt}(-\Delta\omega_r) + 2\left(\frac{2}{n}\right)^2 B_m\omega_0(-\Delta\omega_r) + \frac{2}{n}T_{l0}(-\Delta\omega_r)\right] \tag{17}$$

where k_p is the proportional gain. With this type of modulation for the applied frequency, the simplified small-signal dynamics model given in Fig. 7 can be drawn as shown in Fig. 8.

The block diagram in Fig. 8 gives the characteristic equation for the system as

$$s^2 + \left(\frac{B_m}{J} + \frac{2k_e\omega_0k_p}{n}\right)s + \frac{k_e}{2J}\left[n + \left(\frac{8}{n}\right)B_mk_p\omega_0 + 2T_{l0}k_p\right] = 0. \tag{18}$$

It can be seen from (18) that the damping of the system poles can be controlled by properly selecting the gain k_p. The root locus analysis made for the characteristic (18) shows that keeping the ω_0k_p term constant, i.e., changing the k_p inversely proportional to the rotor speed, an almost constant damping factor (a constant real part for the system poles) can be obtained. This reveals that the location of the machine rotor poles in the s plane can be controlled using the gain k_p when the applied frequency is modulated according to (17).

B. Stability Verification Using Full Small-Signal Dynamics Model

The simplified small-signal dynamics model, which has been used for the analysis in Section III-A, is an easy tool to predict how the applied frequency should be modulated to add damping to the system. However, the simplified small-signal dynamics model analysis has incorporated some approximations. The predictions made using the simplified small-signal dynamics model for the frequency modulation can be verified from the full linearized PMSM model discussed in Section II-B.

Because of the frequency modulation, ω_e is now a variable. Therefore, to model the system, another state should be added to the system (7)–(10) of Section II-B.

Referring to (17), the applied frequency should be modulated as

$$\Delta\omega_e = -k_p\Delta p_e. \tag{19}$$

Δp_e can be extracted by passing the input power p_e through a first-order high-pass filter. Therefore, Δp_e can be written as

$$\Delta p_e = \frac{s}{s + \frac{1}{\tau_h}}p_e \tag{20}$$

where τ_h is the high-pass filter time constant. Substituting Δp_e from (20) in (19), one obtains

$$p\Delta\omega_e + \frac{\Delta\omega_e}{\tau_h} = -k_pp(p_e). \tag{21}$$

The input power to the machine can be written as

$$p_e = \frac{3}{2}[v_{qs}^ri_{qs}^r + v_{ds}^ri_{ds}^r] = \frac{3}{2}V_s[i_{qs}^r\cos\delta - i_{ds}^r\sin\delta]. \tag{22}$$

Taking the derivative for both sides of (22), one obtains

$$p(p_e) = \frac{3}{2}V_s[\cos\delta pi_{qs}^r - \sin\delta pi_{ds}^r - (i_{qs}^r\sin\delta + i_{ds}^r\cos\delta)p\delta]. \tag{23}$$

Substituting $p(p_e)$ from (23) into (21) one can obtain the required fifth state equation for the system.

Now, the five linearized system equations have the form

$$p\Delta x' = A'(X)\Delta x' + B'(X)\Delta T_l \tag{24}$$

where

$$\Delta x' = [\,\Delta i_{qs}^r \quad \Delta i_{ds}^r \quad \Delta\omega_r \quad \Delta\delta \quad \Delta\omega_e\,]^T \tag{25}$$

$$B'(X) = [\,0 \quad 0 \quad \tfrac{-n}{2J} \quad 0 \quad 0\,]^T. \tag{26}$$

The elements of the new state transition matrix $A'(X)$ are given in Appendix III.

The eigenvalues of $A'(X)$ can be used to see the effectiveness of the stabilizing loop, which modulates the applied frequency of the system. Fig. 9 shows the rotor poles of the system, which are obtained from $A'(X)$, under different load conditions as a function of the applied frequency. For the plots shown in Fig. 9, the cutoff frequency of the high-pass filter, which is needed for power perturbation extraction, is selected as 2.5 Hz (i.e., $\tau_h = 0.064$ s) and the gain for the stabilizing loop is calculated as $k_p = 8/\omega_0$ for $\omega_0 \neq 0$. Comparing Fig. 9 with Fig. 6, the added damping to the system from the stabilizing loop is evident.

C. Implementation of the Stabilizing Loop

To implement the stabilizing loop, the frequency modulation signal $\Delta\omega_e$ should be derived using the input power perturbations in the system as given in (19).

The input power to the machine is given by

$$p_e = \frac{3}{2}v_si_s\cos\phi. \tag{27}$$

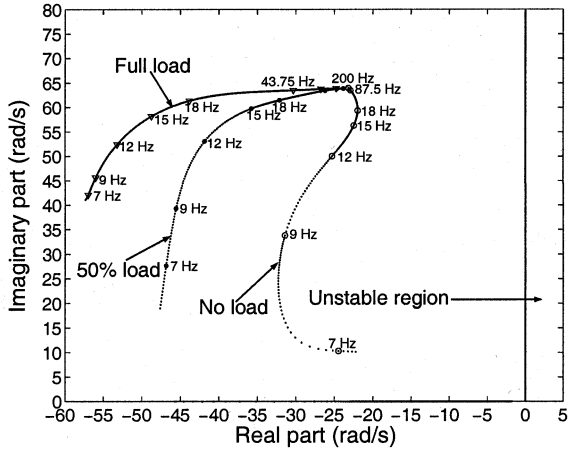

Fig. 9. Loci of the rotor poles under different load conditions, as a function of the applied frequency, with the frequency-modulated stabilizing loop in the system.

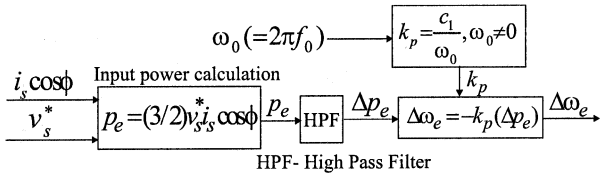

Fig. 10. Derivation of the frequency modulation signal $\Delta\omega_e$.

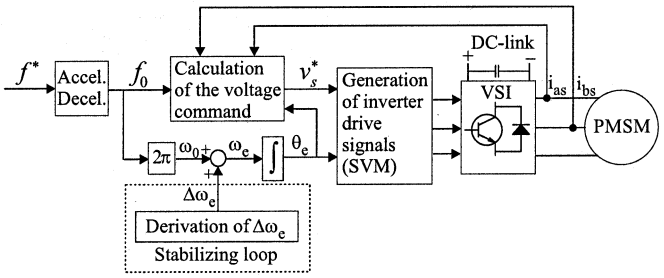

Fig. 11. Complete drive scheme with the stabilizing loop.

The $i_s \cos\phi$ term, which is used to calculate the voltage command in (6) and expressed in (4), and the commanded voltage reference to the machine v_s^* can be used in (27) to calculate the input power. As explained in Section III-B, a first-order high-pass filter can be used to extract the perturbations in the input power. With this knowledge, the derivation of the frequency modulation signal $\Delta\omega_e$ is shown in Fig. 10. The implementation of the full drive scheme with the stabilizing loop is shown in Fig. 11.

IV. Experimental Results

A. The Laboratory Test System

To verify the performance of the drive, the laboratory test system as shown in Fig. 12 is employed. The control algorithm of the drive is implemented in a digital signal processor (DSP) (Analog Devices 21062 SHARC), which can be programmed using C language. The calculated pulsewidth-modulation (PWM) duty cycles in the DSP are passed to a microcontroller

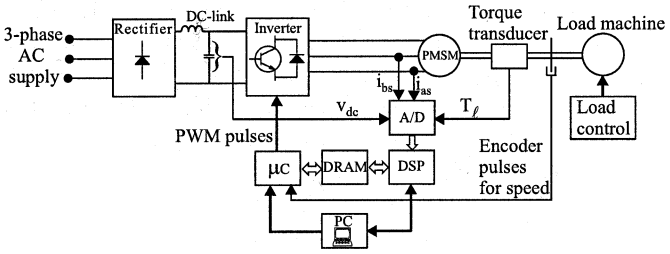

Fig. 12. Laboratory test system.

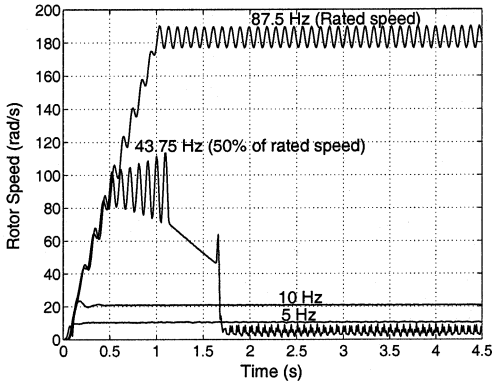

Fig. 13. Measured rotor speeds at different frequencies, under no load, without stabilizing loop in the system.

(μc) (Siemens C167) through the dual-port RAM (DRAM). The μc generates the PWM pulses for the inverter. Moreover, it also counts the encoder pulses to calculate the rotor speed of the PMSM. The sampling frequency and the PWM switching frequency of the system is 5 kHz.

B. Performance of the Drive

In all the experimental results presented in this section, the machine was started after aligning the rotor to a known position and applying the initial voltage vector along the rotor q^r axis, in order to assure a positive starting torque from the machine. The rotor was aligned to a known position applying a dc voltage to the machine as described in [5]. Without knowing the initial rotor position, arbitrarily applying the initial voltage vector to the machine, in some situations, the rotor may rotate in the opposite direction and the smooth start of the machine may not be possible.

Fig. 13 shows the measured rotor speed of the machine, when the machine is ramped up to different frequencies under no load, from the drive configuration shown in Fig. 4, i.e., without the stabilizing loop in the system. From Fig. 13, the stable operation of the machine at low frequencies and the unstable operation at high frequencies is evident, as expected from the stability analysis in Section II-B.

The same test was carried out with the drive configuration shown in Fig. 11, i.e., with the stabilizing loop in the system. The stabilizing loop parameters which were used to calculate the eigenvalue plots in Fig. 9 were used in the drive system. Since the stable operation of the machine was possible at low frequencies the stabilizing loop was added to the system after exceeding

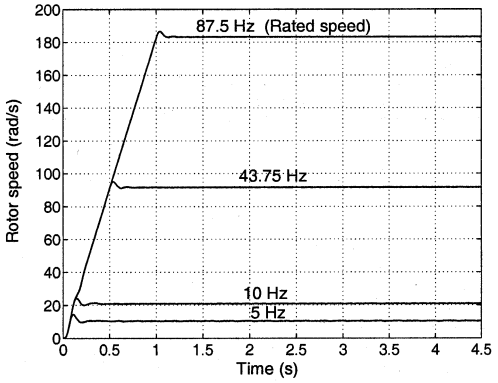

Fig. 14. Measured rotor speeds at different frequencies, under no load, with stabilizing loop in the system.

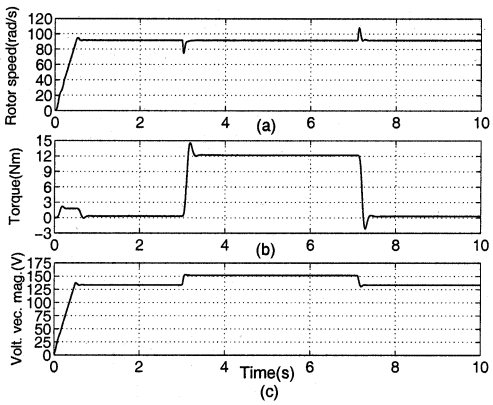

Fig. 15. Measured variables with a 100% load step to the drive at 50% of the rated speed. (a) Rotor speed. (b) Measured torque on the rotor shaft. (c) Commanded magnitude of the voltage vector.

the applied frequency of 3 Hz. Fig. 14 shows the results. Comparing Figs. 13 and 14, the effectiveness of the stabilizing loop in the system can be seen.

Figs. 15 and 16 show the measured variables from the proposed drive system with stabilizing loop, when adding a 12-N·m load step (100% load step) to the machine at 43.8 Hz (50% of the rated frequency). The results in these two figures indicate the drive's capability of overcoming a sudden load change in the system.

To verify the importance of the r_s voltage drop compensation (especially at low frequencies) in the voltage control of the machine, two tests were carried out. For the first test, the complete drive configuration shown in Fig. 11 was used, whereas for the second test only the voltage control of the drive was changed to the relationship given in (3), i.e., voltage control without r_s voltage drop compensation. Both tests were done at 4.4 Hz (5% of the rated frequency) with 50% load step. The measurements are shown in Figs. 17 and 18, respectively. It can be seen from Fig. 18 that the drive cannot overcome the load change due to the lack of voltage to the machine.

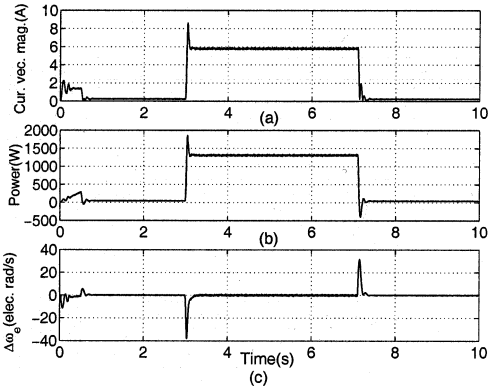

Fig. 16. Measured variables with a 100% load step to the drive at 50% of the rated speed. (a) Magnitude of the current vector. (b) Input power. (c) Frequency modulation signal $\Delta\omega_e$.

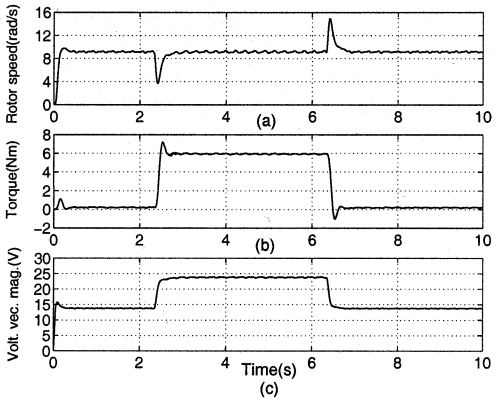

Fig. 17. Measured variables with a 50% load step to the drive at 5% of the rated speed. (a) Rotor speed. (b) Measured torque on the rotor shaft. (c) Commanded magnitude of the voltage vector.

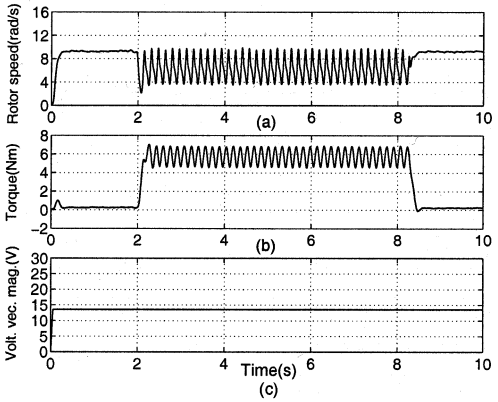

Fig. 18. Measured variables with a 50% load step at 5% of the rated speed, without r_s voltage drop compensation in voltage control of the drive. (a) Rotor speed. (b) Measured torque on the rotor shaft. (c) Commanded magnitude of the voltage vector.

V. Conclusions

The PMSM without damper windings in the rotor becomes unstable after exceeding a certain applied frequency under the proposed voltage control method, which maintains a constant stator flux linkage of the motor. The stable operation for a wide

frequency range can be achieved by modulating the applied frequency proportional to the perturbations in the input power. The simplified small-signal dynamics model, which models only the rotor poles of the PMSM, has shown how to select the gain for this frequency-modulated stabilizing loop. To implement this stabilizing loop, no rotor position sensor or other type of extra sensor is required. This stabilizing loop in the system can also be seen as a signal, which provides synchronization between the machine's excitation frequency and the rotor frequency. Experimental results have shown that from the proposed sensorless, stable V/f control method the drive can operate at 5%-100% of rated speed with the required performance for pump and fan applications.

Appendix I
Calculation of Steady-State Machine Variables for Constant Stator Flux Linkage Control

The magnitude of the stator flux linkage vector

$$\lambda_s = \sqrt{(\lambda_{qs}^r)^2 + (\lambda_{ds}^r)^2} = \sqrt{(L_q I_{qs}^r)^2 + (L_d I_{ds}^r + \lambda_m)^2}. \tag{28}$$

The rotor frame current components can be written from current vector magnitude and torque angle α_0 as (see Fig. 2)

$$I_{qs}^r = I_s \sin\alpha_0 \tag{29}$$
$$I_{ds}^r = I_s \cos\alpha_0. \tag{30}$$

Substituting $\lambda_s = \lambda_m$, putting (29) and (30) into (28), α_0 can be obtained for constant stator flux linkage λ_m as

$$\alpha_0 = \cos^{-1}\left[\frac{-\lambda_m}{I_s L_d(1-\sigma^2)} - \sqrt{\left(\frac{\lambda_m}{I_s L_d(1-\sigma^2)}\right)^2 - \frac{\sigma^2}{(1-\sigma^2)}}\right] \tag{31}$$

where $\sigma = L_q/L_d$ (note that $\sigma > 1$ for an interior-type PMSM). For a given current magnitude I_s, α_0 can be calculated from (31) for constant stator flux linkage λ_m. Knowing I_s and α_0, I_{qs}^r and I_{ds}^r can be obtained from (29) and (30). Then, the torque can be calculated from

$$T_e = \frac{3}{2}\frac{n}{2}[\lambda_m I_{qs}^r + (L_d - L_q) I_{ds}^r I_{qs}^r] \tag{32}$$

and the voltages for a given frequency can be calculated from

$$V_{qs}^r = V_s \cos\delta_0 = r_s I_{qs}^r + \omega_0 L_d I_{ds}^r + \omega_0 \lambda_m \tag{33}$$
$$V_{ds}^r = -V_s \sin\delta_0 = r_s I_{ds}^r - \omega_0 L_q I_{qs}^r. \tag{34}$$

Appendix II
PMSM Parameters

Rated power $= 2.2$ kW;
rated speed $= 1750$ r/min;
rated torque $= 12$ N $\cdot$ m;
number of poles $(n) = 6$;
rated phase-to- phase voltage $= 380$ V(rms);
rated phase current $= 4.1$ A(rms);
$r_s = 3.3\ \Omega$;
$L_d = 41.59$ mH;
$L_q = 57.06$ mH;
$\lambda_m = 0.4832\ \text{V} \cdot \text{s} \cdot \text{rad}^{-1}$;
$J = 10.07 \times 10^{-3}\ \text{kg} \cdot \text{m}^2$;
$B_m = 20.44 \times 10^{-4}\ \text{N} \cdot \text{m} \cdot \text{s} \cdot \text{rad}^{-1}$.

Appendix III
Elements of Matrix $A'(X)$ in (24)

$$\begin{aligned}
A'_{11} &= -1/\sigma\tau_s \\
A'_{12} &= -\omega_0/\sigma \\
A'_{13} &= -1/\sigma\,(\lambda_m/L_d + I_{ds}^r) \\
A'_{14} &= -V_s \sin(\delta_0)/\sigma L_d \\
A'_{15} &= 0 \\
A'_{21} &= \sigma\omega_0 \\
A'_{22} &= -1/\tau_s \\
A'_{23} &= \sigma I_{qs}^r \\
A'_{24} &= -V_s \cos(\delta_0)/L_d \\
A'_{25} &= 0 \\
A'_{31} &= 3/2J\,(n/2)^2\,[\lambda_m + L_d(1-\sigma) I_{ds}^r] \\
A'_{32} &= 3/2J\,(n/2)^2\,L_d(1-\sigma) I_{qs}^r \\
A'_{33} &= -B_m/J \\
A'_{34} &= A'_{35} = 0 \\
A'_{41} &= A'_{42} = 0 \\
A'_{43} &= -1 \\
A'_{44} &= 0 \\
A'_{45} &= 1 \\
A'_{51} &= c\,[\cos(\delta_0)/\sigma\tau_s + \omega_0\sigma\sin(\delta_0)] \\
A'_{52} &= c\,[\omega_0\cos(\delta_0)/\sigma - \sin(\delta_0)/\tau_s] \\
A'_{53} &= c[(\sigma-1) I_{qs}^r \sin(\delta_0) \\
&\quad + 1/\sigma(\lambda_m/L_d + (1-\sigma) I_{ds}^r)\cos(\delta_0)] \\
A'_{54} &= c\left[\left(\omega_0\sigma I_{qs}^r - \frac{1}{\tau_s} I_{ds}^r\right)\cos(\delta_0) - \frac{V_s(\sigma-1)\sin(2\delta_0)}{\sigma L_d}\right. \\
&\quad \left. - \left(\frac{\omega_0}{\sigma}\left(\frac{\lambda_m}{L_d} + I_{ds}^r\right) + \frac{I_{qs}^r}{\sigma\tau_s}\right)\sin(\delta_0)\right] \\
A'_{55} &= c\left[I_{qs}^r \sin(\delta_0) + I_{ds}^r \cos(\delta_0)\right] - 1/\tau_h
\end{aligned}$$

where $\sigma = L_q/L_d$, $\tau_s = L_d/r_s$, $c = 3/2k_pV_s$.

References

[1] P. Thøgersen and F. Blaabjerg, "Adjustable speed drives in the next decade-The next steps in industry and academia," in *Proc. Power Conversion and Intelligent Motion Conf.*, 2000, pp. 95–104.

[2] T. M. Jahns, "Variable frequency permanent magnet AC machine drives," in *Power Electronics and Variable Frequency Drives, Technology and Applications*, B. K. Bose, Ed. Piscataway, NJ: IEEE Press, 1997, ch. 6.

[3] T. Sawa and K. Hamada, "Introduction to the permanent magnet motor market," in *Proc. Energy Efficiency in Motor-Driven Systems Conf.*, 1999, pp. 81–94.

[4] P. Vas, "Vector and direct torque control of synchronous machines," in *Sensorless Vector and Direct Torque Control*. London, U.K.: Oxford Univ. Press, 1998, ch. 3.

[5] N. Matsui, "Sensorless PM brushless DC motor drives," *IEEE Trans. Ind. Electron.*, vol. 43, pp. 300–308, Apr. 1996.

[6] S. Ogasawara and H. Akagi, "Implementation and position control performance of a position-sensorless IPM motor drive system based on magnetic saliency," *IEEE Trans. Ind. Applicat.*, vol. 34, pp. 806–812, July/Aug. 1998.
[7] M. J. Corley and R. D. Lorenz, "Rotor position and velocity estimation for a salient-pole permanent magnet synchronous machine at standstill and high speeds," *IEEE Trans. Ind. Applicat.*, vol. 34, pp. 784–789, July/Aug. 1998.
[8] R. S. Colby and D. W. Novotny, "An efficiency-optimizing permanent-magnet synchronous motor drive," *IEEE Trans. Ind. Applicat.*, vol. 24, pp. 462–469, May/June 1988.
[9] Y. Nakamura, T. Kudo, F. Ishibashi, and S. Hibino, "High-efficiency drive due to power factor control of a permanent magnet synchronous motor," *IEEE Trans. Power Electron.*, vol. 10, pp. 247–253, Mar. 1995.
[10] P. D. Chandana Perera, F. Blaabjerg, J. K. Pedersen, and P. Thøgersen, "Open loop stability and stabilization of permanent magnet synchronous motor drives using DC-link current," in *Proc. IEEE Nordic Workshop on Power and Industrial Electronics*, 2000, pp. 47–53.
[11] I. Boldea, "Driving control without motion sensors," in *Reluctance Synchronous Machines and Drives*. London, U.K.: Oxford Univ. Press, 1996, ch. 7.
[12] A. Munoz-Garcia, T. A. Lipo, and D. W. Novotny, "A new induction motor V/f control method capable of high-performance regulation at low speeds," *IEEE Trans. Ind. Applicat.*, vol. 34, pp. 813–821, July/Aug. 1998.
[13] D. W. Novotny and T. A. Lipo, "d, q modeling of induction and synchronous machines," in *Vector Control and Dynamics of AC Drives*. London, U.K.: Oxford Univ. Press, 1998, ch. 2.
[14] F. Blaabjerg, J. K. Pedersen, and P. Thøgersen, "Improved modulation techniques for PWM-VSI drives," *IEEE Trans. Ind. Electron.*, vol. 44, pp. 87–95, Feb. 1997.
[15] G. C. Verghese, J. H. Lang, and L. F. Casey, "Analysis of instability in electrical machines," *IEEE Trans. Ind. Applicat.*, vol. IA-22, pp. 853–864, Sept./Oct. 1986.
[16] P. C. Krause, O. Wasynczuk, and S. D. Sudhoff, "Linearized equations of induction and synchronous machines," in *Analysis of Electric Machinery*. New York: IEEE Press, 1995, ch. 7.

P. D. Chandana Perera (S'99) was born in Sri Lanka in 1967. He received the B.Sc. degree in electrical engineering from Zhejiang University, Hangzhou City, China, in 1993. He is currently working toward the Ph.D. degree in the Institute of Energy Technology, Aalborg University, Aalborg East, Denmark.

From 1994 to 1997, he was an Engineer in the Electrical Drives Division of Danfoss Industries Ltd., Hong Kong, which was a subsidiary of Danfoss A/S, Denmark. His main research interests are power electronics and control of electric drives.

Mr. Chandana Perera received a Ph.D. fellowship from the Danfoss Professor Programme in 1998.

Frede Blaabjerg (S'86–M'88–SM'97–F'03) was born in Erslev, Denmark, in 1963. He received the M.Sc.E.E. degree from Aalborg University, Aalborg East, Denmark in 1987, and the Ph.D. degree from the Institute of Energy Technology, Aalborg University, in 1995.

He was with ABB-Scandia, Randers, Denmark, from 1987 to 1988. In 1992, he became an Assistant Professor at Aalborg University, where, in 1996, he became an Associate Professor and, in 1998, he became a Full Professor of power electronics and drives. In 2000, he was a Visiting Professor at the University of Padova, Italy, as well as being a part-time Programme Research Leader at the Research Center Risoe in wind turbines. In 2002 he was a Visiting Professor at Curtin University of Technology, Perth, Australia. His research areas are power electronics, static power converters, ac drives, switched reluctance drives, modeling, characterization of power semiconductor devices and simulation, wind turbines, and green-power inverters. He is involved in more than ten research projects with industry, among which is the Danfoss Professor Programme in Power Electronics and Drives. He is the author or coauthor of more than 250 publications on his research topics, including the book *Control in Power Electronics* (New York: Academic, 2002).

Dr. Blaabjerg is a member of the European Power Electronics and Drives Association and the Industrial Drives, Industrial Power Converter, and Power Electronics Devices and Components Committees of the IEEE Industry Applications Society. He is an Associate Editor of the IEEE TRANSACTIONS ON INDUSTRY APPLICATIONS, IEEE TRANSACTIONS ON POWER ELECTRONICS, *Journal of Power Electronics*, and of the Danish journal *Elteknik*. He has served as a member of the Danish Technical Research Council in Denmark since 1997 and, in 2001, he became its Chairman. He is Chairman of the Danish Small Satellite Programme and the Center Contract Committee, which support collaboration between universities and industry. He became a member of the Danish Academy of Technical Science in 2001. In 2002, he became a member of the Board of the Danish Research Councils. He received the 1995 Angelos Award for his contribution to modulation technique and control of electric drives, and an Annual Teacher Prize from Aalborg University, also in 1995. In 1998, he received the Outstanding Young Power Electronics Engineer Award from the IEEE Power Electronics Society. He has received four IEEE Prize Paper Awards during the last five years. He received the C. Y. O'Connor Fellowship 2002 from Perth, Australia.

John K. Pedersen (M'91–SM'00) was born in Holstebro, Denmark, in 1959. He received the B.Sc. E.E. degree from Aalborg University, Aalborg East, Denmark.

He was with the Institute of Energy Technology, Aalborg University, as a Teaching Assistant from 1983 to 1984, and as an Assistant Professor from 1984 to 1989. He has been an Associate Professor since 1989. He is also the Head of the Institute of Energy Technology. His research areas are power electronics, power converters, and electrical drive systems, including modeling, simulation, and design with a focus on optimized efficiency.

Mr. Pedersen received the 1992 Angelos Award for his contribution to the control of induction machines. In 1998, he received an IEEE TRANSACTIONS ON POWER ELECTRONICS Prize Paper Award for the best paper published in 1997.

Paul Thøgersen (M'92–SM'01) was born in Thy, Denmark, in 1959. He received the M.sc.E.E. and Ph.D. degrees from Aalborg University, Aalborg East, Denmark, in 1984 and 1989, respectively.

He was an Assistant Professor at Aalborg University from 1988 to 1991. Since 1991, he has been with Danfoss Drives A/S, Graasten, Denmark, first as an R&D Engineer and, since 1998, as Manager of Control Engineering. His research areas are frequency converters and control and simulation of ac drives. His relationship with Aalborg University has been continued through participation in a number of Ph.D. project steering committees and as the responsible Danfoss Drives Manager of the Danfoss Professor Programme.

Dr. Thøgersen is a member of the European Power Electronics and Drives Association. He received the Angelo Award in 1999 for his contributions to the development of industrial drives.